International Journal of Mechanical and Industrial Technology ISSN 2348-7593 (Online)
Vol. 3, Issue 1, pp: (258-268), Month: April 2015 - September 2015, Available at: www.researchpublish.com

Design, Fabrication, Characterization and Deformation Studies of Fly ash/SiC Reinforced AA2024 Composites

[1]Jaafar Mohammed Yadeem, [2]Gopi Krishna

[1,2] Department Of Mechanical Engineering University College Of Engineering & Technology Acharya Nagarjuna University Nagarjunanagar:: Guntur::Andhra Pradesh, 522 510 A.P., India.

Abstract: **There has been an increasing interest in composites containing low density and low cost reinforcements. So far most of the research work have been carried out by incorporating hard ceramic particles such as Al2O3, SiC, Flyash and graphite particles to soft matrix like pure aluminium, A2024, A356, A6061 and many more alloys and very few worked on combination of reinforcements (hybrid composites). In the current work, an attempt has been made by combining two types of ceramic particles like flyash and silicon carbide in equal proportions for preparation of hybrid composites, which significantly improves the mechanical properties and wear properties of the Aluminum based MMCs.**

Experiments have been conducted under laboratory condition to assess the mechanical characteristics of the aluminium FA/and SiC composite under different size particle conditions. This has been possible by fabricating the samples through usual stir casting technique. To enhance the mechanical properties the surfaces of the samples were studied under optical microscope to get an idea about the effect of particulate reinforcement on the micro structure behavior of the composite. Dispersion of FA and SiC particles in aluminium matrix A2024 improves the hardness of the matrix material and also the mechanical behavior of the composite .

Dry sliding wear tests on a pin-on-disc apparatus show the resistance to wear increase with increasing FA and SiC content. The alloy exhibited higher wear and the composite with 15% wt fraction showed lower wear. A decrease in the coefficient of friction (μ) for both the alloy and composites was observed with increase in the applied load as well as reinforcement content.

Keywords: **Composite Materials, Fabrication Facilities, Friction And Ring Compression Test, Microstructure and Mechanical properties of Flyash/SiC Particles Reinforced AA 2024 Hybrid Composites, Dry Sliding Wear Behaviour Of flyash/Sic Particles Reinforced Aa 2024 Hybrid Composites Fly Ash Particles Reinforced AA 2024 Composites.**

I. INTRODUCTION

1.1 Composite Materials:

The term composite material has many meanings based on various literatures; one of them is the combination of different multifunctional material systems that provide excellent properties which are not possible in individual systems.

Initial investigations were made with process development using fiber reinforcement. Anisotropy, expensive fabrication cost and restricted secondary processing has led to the use of short fiber / particulate / whisker reinforced composites. The combination of good transverse properties, low cost high workability and significant increase in performance over unreinforced alloys are the commercially attractive features of these discontinuous reinforced composites. Compared to dispersion strengthened systems, particulate reinforced composites contain coarse size reinforcement (1-100 μm) in

relatively high weight fractions (1-30%). In particulate composites, both matrix and reinforcement bear substantial load. In addition, matrix strength as affected by precipitation and dislocation strengthening plays an important role in the load bearing capacity of these composites. Metal matrix composites reinforced with ceramic particles are widely used due to their high specific modulus, strength and wear resistance.

1.2 Classification of Composites:

In general, composites are classified according to the type of matrix material and the nature of reinforcement at two distinct levels. The first classification includes [1] ceramic matrix composites (CMCs) organic matrix composites (OMCs) and metal matrix composites (MMCs). The term organic-matrix composite is generally assumed to include polymer matrix composites PMCs) and carbon matrix composites. The second classification refers to the reinforcement form; particulate reinforcements, whiskers, continuous fiber, laminated composites and woven composites.

COMPOSITES can be classified into:

1. Polymer Matrix Composites (PMCs)

2. Ceramic Matrix Composites (CMCs)

3. Metal Matrix Composites

1.3 Processing Of Composites:

Composites are manufactured through different routes i.e., solid state processing, liquid metallurgy, two phase processing and in-situ –processing. Table 1.2 briefs various systems and the processing routes. Reinforcement distribution is a major factor in deciding the microstructure which intern dictates the mechanical properties. Proper mixing methods can minimize the agglomeration of the reinforcement and setting of the particles can be minimized by quick pouring and employing chill casting technique. Secondary processing like rolling, forging, and extrusion give better distribution of reinforcements. SiC in various forms has been the most widely used reinforcement, in aluminum alloy. Other reinforcements are A12O3, SiO2, TiC, TiO2, ZrO2, borate whiskers, quartz, diamond, graphite, fly ash etc Among the various metal matrix composites (MMC), aluminum alloy metal matrix composites have successfully demonstrated their potential for even high volume applications.

II. FABRICATION FACILITIES

2.1 Furnace:

In the present investigation, preparation of alloys and fabrication of composites were carried out in pot furnace, furnace details were given below.

Figure 2.1 Pot furnace, with a stirrer

2. 2 TESTING FACILITIES:

A. Physical Testing:

1. Optical Microscopy
2. SEM and EDS
3. XRD
4. Density and Porosity

B. Mechanical Testing:

1. Hardness
2. Tensile And Compression
3. Ring Compression Test
4. Wear Test

1. Hardness:

Vickers microhardness studies were carried out for the investigated materials using vickers microhardness tester (Model: UHL IMS 4.0), and Leco vickers hardness tester (Model: LV 700, USA) with 1kg load. The indentation time for the hardness measurement was 15 seconds. An average of six readings was taken for each hardness value.

2. Tensile And Compression:

Tensile strength and compression strength of alloy and composites at room temperature was determined using a computer controlled 100kN DAK universal testing machine. Compression tests were carried out on cylindrical specimens. These cylindrical specimens of standard dimensions were prepared using conventional machining operations of turning and facing. Specimen edges were chamfered to minimize folding. Concentric v- grooves of 0.5mm deep were made on the flat surfaces to have a low friction between die and work piece during compression. Standard specimens of sizes Ø 12mm×12mm (Ho/Do=1.0) and Ø 18mm×12mm (Ho/Do= 1.5) are upset by placing between the flat platens at a constant cross head speed of 0.3mm/min in dry conditions.

Figure 2-6 Experimental setup of compression test machine

3. Wear Test:

Dry sliding wear tests have been carried out on a pin- on- disc apparatus (Model: Ducom TR- 20 LE, (Figure 2.7) by sliding a cylindrical pin against the surface of hardened steel disc (with a hardness value of HRC 62) under ambient condition. The disc was ground to a smooth surface finish and renewed for each test.

The wear test specimens were prepared from the alloy and composite castings in the dimensions of 4 mm and 30 mm length. Prior to testing, test samples were polished with emery papers and cleaned in acetone, dried and then weighed using an electronic balance (Model: lyco balance) having a resolution of 0.1 mg.

III. FRICTION AND RING COMPRESSION TEST

3.1 Friction and Ring Compression Test:

Friction is the resistance to motion encountered when one body slides over another. In metal working processes it arises from sliding of the work piece against the die [1]. In the interest of clarity, friction forces are often neglected. In many real metal working processes friction is the predominant factor [2]. Shaw et al. [3] discussed the significance of axisymmetric compression, and then the mechanical/manufacturing properties of materials, to estimate forming limits up to plastic instability and fracture. Considerable attention has been devoted to the analysis of platen forces and pressure distributions in upsetting, particularly for thin discs [4-8].

$$\tau_i = m\frac{\sigma_o}{\sqrt{3}}$$

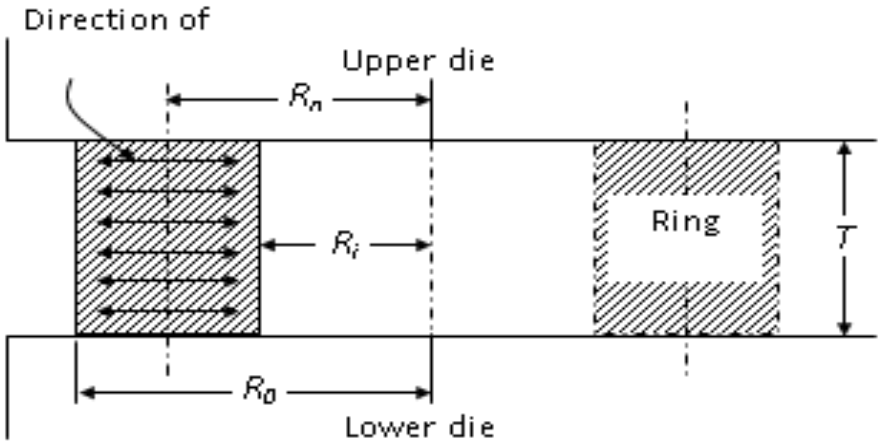

Figure 3-1: Compression of flat ring-shaped specimen between flat dies.

Neither the basic yield stress of the material, σ_0, nor the interfacial shear stress, τ, appear in the final equations in terms of absolute values, only as a ratio, *m*. The basic assumption in the analysis is that this ratio remains constant for the material and deformation conditions. If the analysis is carried out for a small increment of deformation, σ_0 and τ can be assumed to be approximately constant for this increment and the solution is valid. Thus, if the shear factor *m* is constant for the whole operation, it would appear justifiable to continue the mathematical analysis in a series of small deformation increments using the final ring geometry from one increment as the initial geometry for the subsequent increment and so on. As long as the ratio of the interfacial shear stress, τ, and the material flow stress, σ_0, remained constant it would not be of consequence if the ring material strain hardened during deformation provided that the increase in work hardening in any one single deformation increment could be neglected. The progressive increase in interfacial shear stress accompanying strain hardening would also be of no consequence provided that it could be assumed to be constant over the entire die/ring interface during any one deformation increment. Thus it is possible that the analysis could be justifiably applied to real materials even though it was initially assumed that the material would behave according to the Mises' stress-strain rate laws provided that the assumption of a constant interfacial shear factor, *m*, is correct.

$$\mu = F/R = \tau_i / p = \tau_i / \text{hardness}$$

Where: F = force of friction, R = normal reaction, p = interface pressure $\cong \sigma_0$, and τ_i = interface shear stress.

3.2 Compression Testing of Short Cylinders:

The compression of a short cylinder between anvils is a much better test for measuring the flow stress in metal working applications [9-11]. The nature of tensile instability due to necking can be avoided and the test can be carried out to

strains in excess of 2.0 (for ductile material). Friction between the specimen and anvils play key role. In the homogeneous upset (zero friction) test a cylinder of diameter D_0 and initial height H_0 would be compressed in height to H and spread out in diameter to D according to the law of constancy of volume.

$D_0^2 H_0 = D^2 H$

IV. MICROSTRUCTURE AND MECHANICAL PROPERTIES OF FLYASH/SIC PARTICLES REINFORCED AA 2024 HYBRID COMPOSITES

4.1 Materials And Methods Casting of A2024 alloy:

Pure aluminium (99.5+ % EC grade) was procured from M/s HINDALCO as 20 kg ingots, bus-bars of conductivity grade copper (99.95% Cu) and the ingot of high purity magnesium (99.9+%) were purchased from local market. Cut ingots of pure aluminium were melted in a stationary pot type electric heating furnace in a graphite crucible at 700ºC. In order to prevent excess oxidation of the metal Coverall (0.1 wt% of metal) proprietary covering agent, supplied by M/s Fosceco (I) Ltd wss used. Magnesium in the form of thin slices wrapped with aluminium foil was added to the Al-Cu alloy melt after the furnace temperature was reduced to 700ºC. Magnesium oxidation was minimized by plunging the Magnesium slices to the bottom of the melt and allowed to melt then itself. Melt was well mixed with a graphite sheathed tube for uniformity in composition. A small amount of Coverall was once again added to the melt. Once the pouring temperature attained the metal was thoroughly degassed using Argon for one minute. The top layer was skimmed and metal was cast into a preheated (200O C) S.G. iron mould of 180 mm x 18 mm Φ cylindrical fingers. Homogenization treatment was carried out at 200 0C for 24hrs to relieve the internal stresses and minimize the chemical inhomogenities which may be present in the cast alloys. The chemical composition of A2024 was shown in table 1; the same was carried out by using X-MET 3000 TX equipment.

4.2 Fabrication Of Composites:

In the present investigation, aluminium based hybrid metal matrix composites containing 5, 10 and 15wt% SiC and Flyash particulates of 70µm were successfully synthesized by vortex method. The matrix materials used in this study was Al-Cu-Mg alloy (AA 2024) whose chemical composition was shown in table 4-1..

4.3: Characterization Of Composites Metallography and Hardness tests:

Scanning electron microscopy ((Model: SEM – Hitachi S-3400N - Japan) with EDAX energy dispersive X-ray spectroscopy (EDS) was used in order to evaluate the morphological changes and the elemental analysis of the alloy and the composites. The hardness of the alloy and composite was evaluated by using Leco Vickers hardness tester (Model: LV 700- USA). An average of ten readings was taken for each hardness value.

Density And Porosity Tests:

The density of the alloy and composites was measured by the Archimedes drainage method by using the following equation:

$$\rho_{MMC} = (m)/(m - m_1) * \rho_{H20} \quad \text{.....4-1}$$

Where ρMMC is the density of the composite, ‘m’ is the mass of the composite sample in air, ‘m1’ is the mass of the same composite sample in distilled water and ‘ρH2O’ is the density of distilled water (at 293K) is 998 kg/m3. Theoretical density calculations, according to the rule of mixture were also used to determine the densities of the composites. This was obtained from the below equation.

$\rho_c = V_r\rho_r + (1\text{-}V_r)\,\rho m$

Microstructures and EDS of alloy and composites:

Figure 1 (a-f) shows the SEM and optical micrographs of flyash particles, X-ray diffractograph and hybrid composites varying with wt. percentages of 5 to 15%. We can observe that, addition of fly ash and SiC in the alloy, i.e. by increasing the fly ash and SiC by weight percent the increased percentage conte nt can be seen clearly by using the Olympus- 5060-G x 4, Japan, fig (c) shows the the microstructure of the SEM Micrograph of Flyash particles.

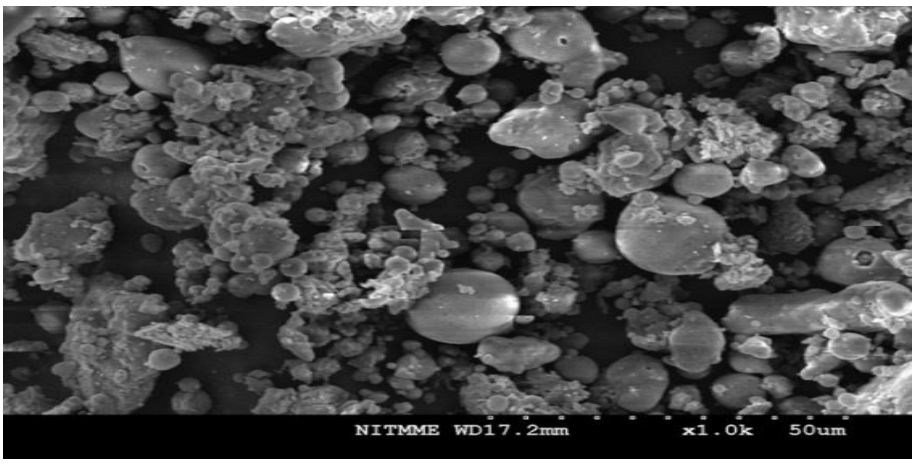

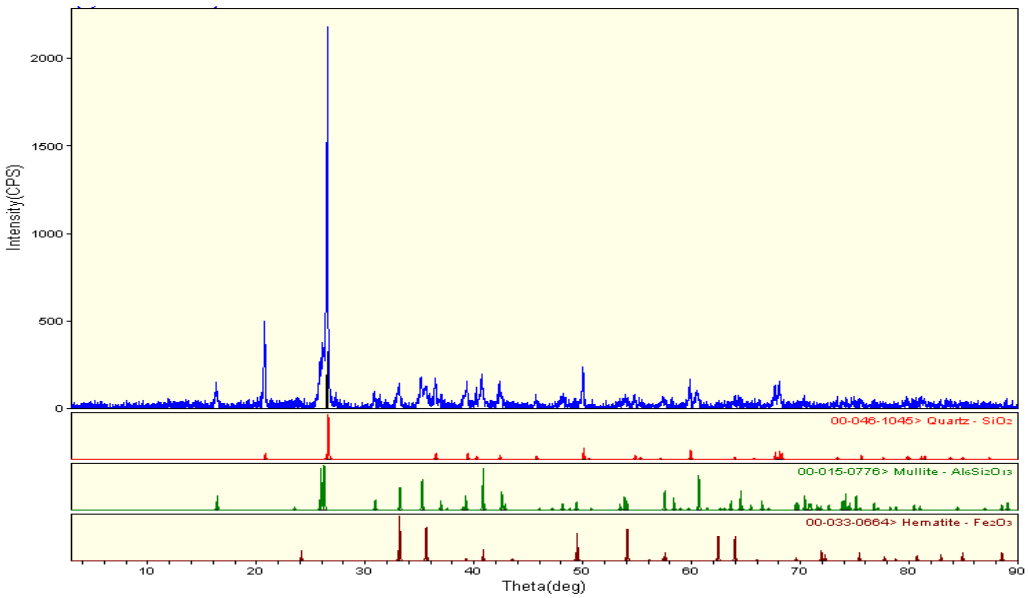

X-ray diffractogram of fly ash particles

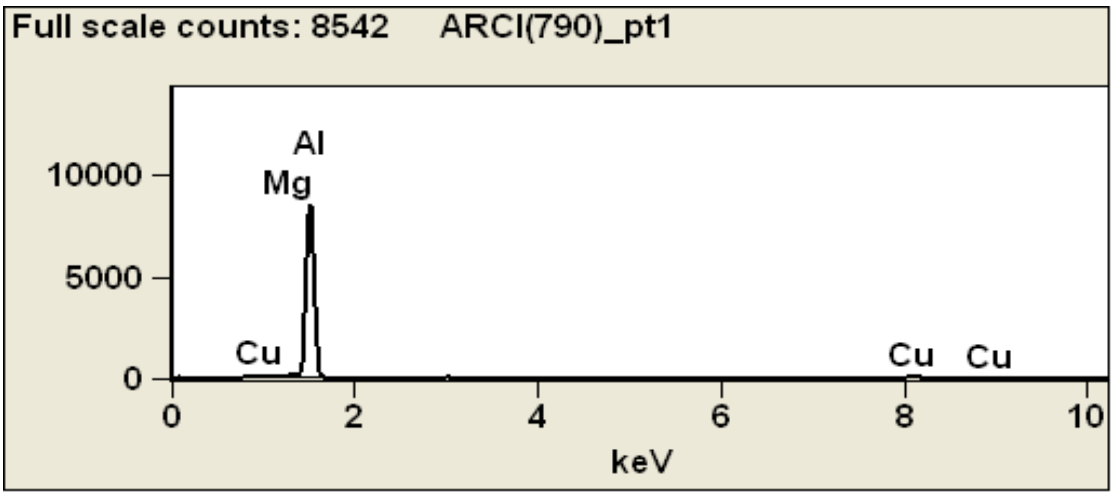

	Mg-K	*Al-K*	*Cu-K*
ARCI(790)_pt1	**1.17**	**92.84**	**5.98**
ARCI(790)_pt1	**+/-0.13**	**+/-0.46**	**+/-0.60**

Figure 4-2 EDS spectrum on the matrix phase

4.8 Conclusions:

1. Thebulkdensityoftheflyashparticleswasfoundtobe2.42g/cm3.

2. A2024/FA/SiC Hybrid composites were produced by stir casting route successfully.

3 .There was a uniform distribution of FA/SiCp article sin the matrix phase.

4FromtheSEMfigures,it clearly shows that there were no voids and discontinuities in the composites; there was ago od inter facial bonding between the FA/SiC particles and matrix phase.

5. The density of the composites decreases within creasing the percentage so fFA /SiC particulates compared to the density of the alloy2.680g/cm3.

6 .The measured densities were lower than that obtained from theoretical calculations. The extent of deviation increases within creasing FA/SiC content .

7. From the EDX analysis of composites shows that no oxygen peaks were observed in the matrix area, confirming that the fabricated composite did not contain any additional contamination from the atmosphere. This might be due to a shield of argon gas was maintained during the mechanical stirring while rein for cement addition.

8. The hardness of the composite sin creased with increasing the amount of FA/SiC than the base alloy.

V. EXPERIMENTAL STRESS ANALYSIS OF OF FLYASH/SICPARTICLESREINFORCED AA 2024 HYBRID COMPOSITES

5.1 Computation Of Plastic Strain:

Plastic strain (ε_p) = (Total strain) – $\left(\frac{\text{Stress}}{\text{Young's modulus}}\right)$

From figure 5-1 $C = y - mx = \bar{\sigma} - E\varepsilon_{tot}$

$$\varepsilon_P = -C/m = \frac{-C}{E} = -\frac{(\bar{\sigma} - E\varepsilon_{tot})}{E}$$

$$\bar{\varepsilon} = \varepsilon_P = \varepsilon_{tot} - \frac{\bar{\sigma}}{E} \ldots$$

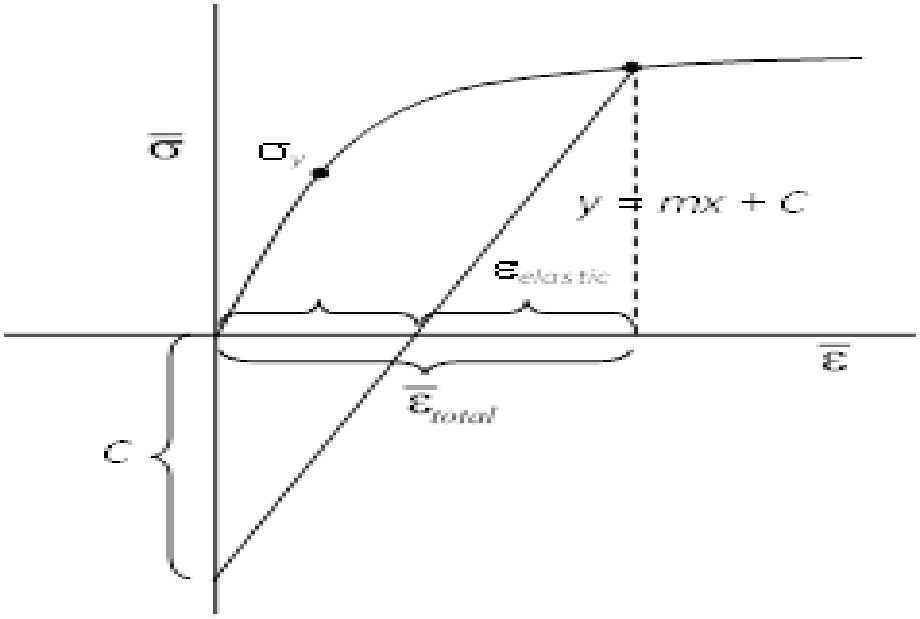

Figure 5-1 Elastic and plastic components of total strain

5.2 Optical Measurements Of Strains:

Knowledge of material behaviour requires the measurement of mechanical parameters. Strains are usually measured by the use of strain gauges. When the specimen is distant, difficult to reach, in a hostile environment or does not support the attachment of gauges, the use of measurement techniques without contact such as optical methods, allows to determining the desired parameters. These non-contact and non-destructive methods can represent a real advance for displacement, stress and strain measurements. There are two types of experimental methods for strain measurement, indirect and direct methods. Indirect techniques allow strains to be determined by derivation of the measured displacement field. Among indirect methods the principles of ones include digital image correlation [12], speckle interferometry [13] or Morié techniques [14]. Direct methods give strains using an extensometer, gauges, three element rosettes or grid [15-17]. All these tools can only be used for strains less than 20% and also do not allow the measurement of larger deformation. Three optical methods can be employed for large strain measurement using a grid (lines or spots) method of mark-tracking techniques.

5.3 Theoretical Background Of Orthogonal Axes:

The orthogonal axes of reference for the component of stress and strain increment on the free surface of a compression specimen are as shown in figure 5-2. It is assumed that throughout the compression test the principal axed of stress and strain increment coincide. The reference axis, r, in a principal direction because the shear stresses on a free surface are zero, and θ-axis is principal direction because the flow is symmetrical about the longitudinal axis, hence the z-axis is also a principal direction.

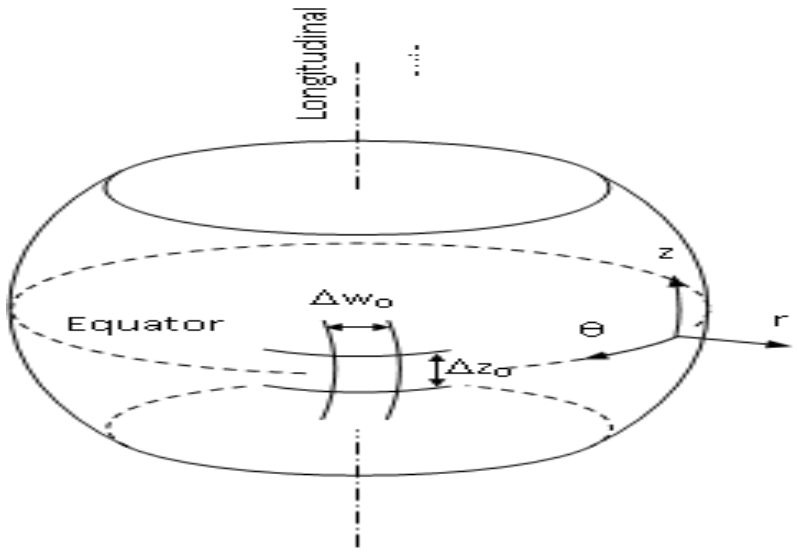

Figure 5-2 Showing the orthogonal axes of reference

5.4 Experimental Details:

1. Ring Compression Test

2. Experimental Strain Measurements

5.4.2.1 Experimental Set Up:

A PC–based system consisting of a video camera (Logitech charge coupled device) with an integrated digitizing capacity with resolution of 640x480 pixels and 256 colour full depths attached with a magnifying glass was used. The shutter speed used was 20 pictures (full frame) per second and was sufficient enough to record the images as the run speed of the upsetting process was a slow test performed on computer controlled bench mark machine of 100 kN capacity. Figure 5-4 demonstrates the experimental setup.

5.4.2.2 Materials:

The upsetting tests were performed on four different materials viz., AA2024 alloy , and AA2024-2% fly ash, AA2024-6% fly ash and AA2024 –10% fly ash composites in the following conditions.

(i) Aspect ratio (H_0/D_0) of 1.0, and

(ii) Aspect ratio (H_0/D_0) of 1.5.

5.4.2.3 Compression Testing:

The upset tests were performed at room temperature between two flat platens on a computer controlled UTM of 100 kN capacity universal testing machine (Model: UT 9102; Dak System inc). The compression dies of H11 grade are used for compression and the sample is placed axi-symmetrically in between the dies. The tests were conducted at a constant cross head speed for both the alloy and composites for all the specimens. Details of the process control parameters and necessary precautions were discussed in chapter 2. The compression tests were carried out until either 50% reduction in height or initiation of the fracture on the specimen surface whichever is earlier. A PC based data logging system was used to record and store the loads and displacements continuously.

VI. DRY SLIDING WEAR BEHAVIOUR OF OFFLYASH/SIC PARTICLES REINFORCED AA 2024 HYBRID COMPOSITES FLY ASH PARTICLES REINFORCED AA 2024 COMPOSITES

6.1 Types Of Wear:

Wear occurs as a natural consequence when two surfaces with a relative motion interact with each other. Wear may be defined as the progressive loss of material from contacting surfaces in relative motion. Scientists have developed various wear theories in which the Physico-Mechanical characteristics of the materials and the physical, conditions (e.g. the resistance of the rubbing body and the stress state at the contact area) are taken in to consideration. A fundamental scheme to classify wear was first outlined by Burwell and Strang [13]. Later Burwell modified the classification to include five distinct types of wear, namely (a) Abrasive (b) Adhesive (c) Erosive (d) Surface fatigue, and (e) Corrosive.

(a) Abrasive Wear

(b) Adhesive Wear

(c) Erosive Wear

(a) Surface Fatigue Wear

6.2 Experimental Work:

In the present work studies have been carried out to assess the wear behaviour of AA2024-fly ash composites under controlled laboratory conditions. A comprehensive picture of wear under different working conditions has been presented by conducting laboratory tests in pure sliding mode using a pin-on-disc machine; and further characterization was carried out by using scanning electron microscopy to know the wear mechanism.

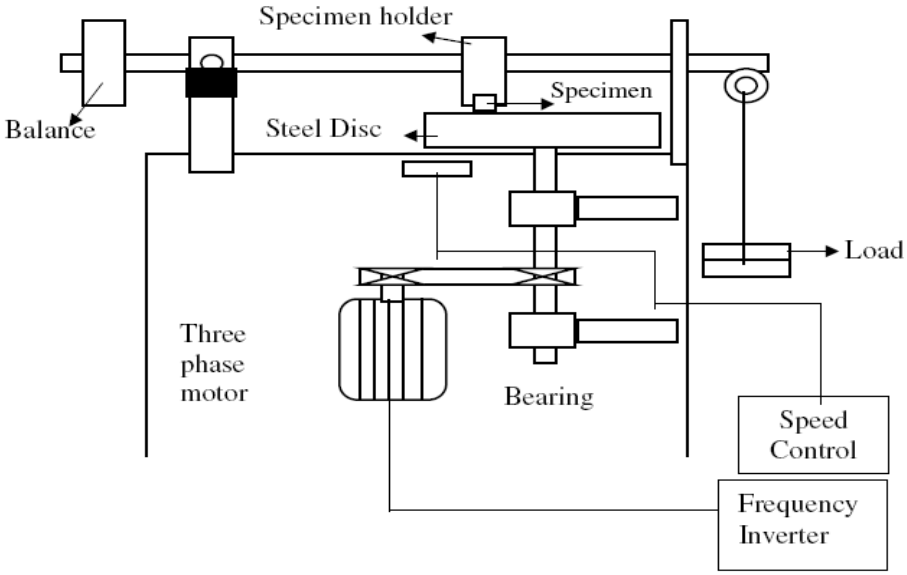

Figure 6.5: Pin-on-disc wear tester (Model: Ducom TR- 20 LE)

6.3 Results And Discussion:

Figure 6.6 shows the sliding wear behavior of AA 2024 alloy and AA 2024 alloy- 2, 6 and 10 wt. % fly ash composites. The normal load applied was 0.5 Kgf. The wear test was conducted for a period of 30 min at a sliding speed of 640 rpm on a steel disc with 120 mm track diameter and the track velocity was 2.0 m/sec. In all the results it was evident that the resistances to wear increases with increasing fly ash content. With increasing fly ash content, the amount of particle present strengthens the matrix and hence more wear resistance was observed. The MMCs with lower weight fractions of fly ash underwent large wears, and the wear increased almost linearly with time. The base metal exhibits higher wear, and the MMCs with 10% fly ash showed lower wear. The presence of hard fly ash particles in AA 2024 alloy matrix might be reason for the lower wear losses for composites compare to base alloy. The sliding wear behavior of base alloy and MMCs for various normal loads of 1.0 kgf and 1.5 kgf was shown in figures 6.7 and 6.8 respectively. The amount of wear increases with increasing normal load. With increasing normal load, MMCs underwent a transition from mild to severe wear.

The change in the friction coefficient (μ) with loads at 0.5 kgf, 1.0 kgf and 1.5 kgf of AA 2024 alloy and AA2024 alloy-2, 6 and10 wt. % fly ash composites were shown in figures 6.9 to 6.11 respectively; also figure 6.12 shows the overall comparison of alloy and the fly ash composites. It was observed that increasing in the applied load as well as fly ash content there was a decrease in the coefficient of friction (μ) for both the alloy and composites. Also it was observed that this decrease in coefficient of friction (μ) was more for higher fly ash content, as shown in figure 6.12. M. Ramachandra et al [18] has also observed the same trend of decreasing the coefficient friction with both the increasing fly ash content and also at higher applied loads. The decrease of coefficient of friction with increase of the load may be attributed to increasing amounts of wear debris particles coming out from the wear surface and filling in the empty spaces between fly ash particles, thereby decrease in the effective depth of penetration. Since the wear debris particles are loose, they can also start sliding at the interface between the pin material and the abrasive causing reduced grooving of the matrix, and also decreasing the effectiveness of the cutting force of fly ash. The loose debris can get in between the rubbing surfaces causing the wear mechanism to change from two-body to three body abrasion. This effect may be more dominant and so it has been able to obliterate the general trend of increase in coefficient friction with load.

Figures 6.13 (a-c) shows the wear rate as a function of sliding distance at 0.5 kgf applied load for AA 2024 alloy and AA 2024 alloy - 2, 6 & 10 wt. % fly ash composites respectively. It was observed that wear rate decreases for alloy with increase in sliding distance from 1.2 km to 2.4 km and then onwards slight increase in wear rate was observed for the sliding distance of 3.6 km. Material under wear process is similar to the plastic deformation phenomenon which leads to cold working of the material. Hence the decrease in wear rate for the material under investigation is due to the strain hardening behaviour of soft α - matrix in the presence of hard $CuAl_2$ (θ) phase in the matrix. Whereas AA2024-fly ash composites shows the lower wear rates for all the sliding distances of 1.2 km, 2.4 km and 3.6 km. Further decrease in wear rate was observed for higher fly ash content in the matrix alloy, the same was revealed in 10% fly ash composite, figure 6.13 (c). This lower wear rate phenomenon of the composites might be due to the presence of hard fly ash particles in the matrix alloy in addition to strain hardening phenomenon of matrix alloy.

For further increasing the applied load from 0.5 kgf to 1.0 kgf marginal increase in wear rate was observed for both the alloy and composites; also lower wear rates were observed for all the composites under investigation than the matrix alloy, as shown in figure 6.14 (a-c). At the applied load of 1.5 kgf decrease in wear rate of the matrix alloy was observed with increasing sliding distances from 1.2 km to 3.6 km; in case of the fly ash composites a reverse phenomenon was observed i.e. there was increase in wear rate with sliding distance, as shown in figure 6.15 (a-c). For lower sliding distances (1.2 km) composites exhibit better wear performance than alloy; however further increase in sliding distances from 2.4 km to 3.6 km composites were the main victim by the wear process. This might be due to the delamination and chipping out of the fly ash particles from the matrix.

ACKNOWLEDGEMENT

I have received generous help from a number of people to carry on my research work. Without their co-operation and encouragement I could not have completed my work. With pleasure I acknowledge my irredeemable debt to them. I am very much thankful to my parents for their encouragement and support for the completion of the present project work.

REFERENCES

[1] Daniel B. Miracle and Steven L. Donaldson, Air force Research Laboratory, pp

[2] S Ray, "Review: Synthesis of cast metal matrix particulate composites", J. Mat. Sci., 1993, Vol.28, pp. 5397-5413.

[3] K.K. Chawla, Composite Materials Science and Engineering, Springer-Verlag New York Inc. 1987.

[4] Lloyd DJ, Aspects of fracture in particulate reinforced metal matrix composites ActaMetall Mater 1991; 39:59–71.

[5] Emmanuel Gikunoo "Effect of Fly Ash Particles on the Mechanical Properties and Microstructure of Aluminium Casting Alloy A535" M.S Thesis, p.97, 2004.

[6] VarunSethi, "Effect of Aging on Abrasive Wear Resistance of Silicon Carbide Particulate Reinforced Aluminum Matrix Composite" M.S Thesis, pp.77-78, 2007.

[7] N Chawla, C. Andres, J.W. Jones, J.E. Allison, Metall. Mater.Trans-A, 29A (1998) pp.2843.

[8] G GSozhamannan, S BalasivanandhaPrabu and V S K Venkatagalapathy "Effect of Processing Paramters on Metal Matrix Composites: Stir Casting Process", Journal of Surface Engineered Materials and Advanced Technology, 2012, 2, pp 11-15.

[9] Hawkyard, J. B., and Johnson, W., "An analysis of the changes in Geometry of a Short Hallow Cylinder During Compression," International J. of Mechanical Sciences, Vol.9; 1967: pp.163.

[10] Betzalel Avitzur "Metal Forming: Processes and Analysis" TMH Edition 1977 Tata McGraw-Hill, Inc. New York.

[11] Schey J.A., T.R.Venner and S.L.Takomana., "The effect of friction on pressure in upsetting at low diameter to height ratios" Journal of Mechanical working technology, Vol 6; 1982: pp. 23-33.

[12] Altan T, Bonlger F.W. "Flow stress of metals and its applications in metal forming analysis" Journal of Engineering Industry, Vol. 95; 1973: pp. 1009-1019.

[13] Bruck, H.A., Mc Neill, S. R., Sutton, M.A. and Peters, W.H. Digital image correlation using Newton-Raphson method of partial differential correction. Exp. Mech., Vol. 29, no.3; 1989: pp. 261-267.

[14] Joenathan, C., Franze, B., Haible, P. and Tiziani H.J. Speckle interferometry with temporal phase evaluation for measuring large-object deformation. Appl. Opt., Vol. [15] no.13; 1998: pp. 2608-2614.

[15] Han, B., Ifju, P. and Post D. Geometric moiré methods with enhanced sensitivity by optical/digital fringe multiplication. Exp. Mech., Vol. 33 no.3; 1993: pp. 195-200.

[16] Sevenhuijsen, P.J. the Development of a laser grating method for the measurement of strain distribution in plane, opaque surface. V.D.I. Berichte, Vol. 313; 1978: pp. 143-147.

[17] Dupre, J.C., Cottron, M. and Lagarde, A. Grating interrogation: from small to large strain measurements. Exp. Mech., Vol. 35 no.2; 1995: pp. 153-157.

[18] Mc Kelvie, J. Moiré strain analysis: an introduction, review and critique, including related techniques and future potential. J. Strain Analysis, Vol. 33, no.2; 1998: pp. 137-151.

[19] Hollomon. J. H, Transactions, AIME, Vol. 162; 1945: pp. 268.